Modeling and Simulation Techniques for the NASA SLS Service Module Panel Separation Event; From Loosely-Coupled Euler to Fully-Coupled 6-DOF, Time-Accurate, Navier-Stokes Methodologies

Leslie H. Hall[1], William M. Eppard[2], Michael P. Applebaum[2], and David C. Purinton[2]
Mclaurin Aerospace, Jacobs ESSCA Group, Huntsville, AL, 35802

An aerodynamic database has been generated for use by the Orion Multi-Purpose Crew Vehicle (MPCV) Program to analyze Service Module (SM) panel jettison from the NASA SLS vehicle. The database is a combination of CFD data for the panel aerodynamic coefficients, and MATLAB code written to query the CFD data. The Cart3D inviscid CFD flow solver was used to generate the panel aerodynamic coefficients for static panel orientations and free stream conditions that can occur during the jettison event. The MATLAB code performs the multivariate interpolation to obtain aerodynamic coefficients. The MATLAB code uses input for SM panel parameters and returns the SM panel aerodynamic force and moment coefficients for use with a Six-Degree-of-Freedom (6-DOF) motion solver to model the jettison event. This paper examines the accuracy of the sequential-static database approach by modeling the panel jettison event with a fully-coupled, time-dependent, viscous, moving-body CFD simulation. The fully-coupled simulation is obtained using the Loci/Chem unstructured Navier-Stokes CFD solver. The results show that the fully-coupled approach agrees well with the loosely-coupled database/6-DOF approach, indicating that unsteady effects are minimal for the panel jettison event. These results suggest that the database/6-DOF approach is sufficient. In addition, this paper presents the development of an uncertainty model for use in Monte Carlo analysis of the panel jettison event. Here viscous CFD simulations are obtained with Loci/Chem and compared to the inviscid CFD forces and moments. An uncertainty model based on model-form error and numerical error is presented.

I. Introduction

SPACE Launch System (SLS) Service Module (SM) panel aerodynamic coefficient database is generated for use by the Orion Multi-Purpose Crew Vehicle (MPCV) Program to analyze the SM panel jettison event for purpose of clearance analysis. The database is a combination of Computational Fluid Dynamic (CFD) data for the panel aerodynamic coefficients, and MATLAB® code written to query the CFD data. The Cart3D[1,2] inviscid CFD flow solver, developed by NASA Ames, was used to generate the panel aerodynamic coefficients during all phases (*i.e.*, hinged, near proximity, and far) of the jettison event. While the CFD data defines the aerodynamics of the SM panel, the MATLAB® code performs the multivariate interpolation, and provides an easy, accurate "black box" approach to obtain aerodynamic coefficients. The MATLAB® code uses input values for the SLS vehicle and SM panel parameters, and returns the SM panel aerodynamic force and moment coefficients for use with a Six-Degree-of-Freedom (6-DOF) motion solver to model the jettisoned event.

Without the availability of experimental or flight data, CFD represents the next most viable option to satisfy the needs of the program for obtaining aerodynamic coefficients for the SM panel jettison event. The Cart3D inviscid solver has been utilized extensively for rapid design and has been well validated. In general, the panel aerodynamic loads are primarily the result of inviscid flow phenomena. Previous analysis[3] during the Ares program shows that inviscid simulations are in good agreement with both Newtonian theory and full Navier-Stokes simulations.

[1] Director of Engineering, Member AIAA.
[2] Senior Research Scientist

The aerodynamic coefficients provided in the database result from static, steady state simulations, and do not include the unsteady effects resulting from panel motion. As a result, use of the SM panel aerodynamic database coupled with a 6-DOF solver represents a "sequential-static" (quasi-unsteady) simulation. In this method, the panels are repositioned at a new time level based upon aerodynamic loads at the previous time level; however, the aerodynamic coefficients do not include the effects of panel motion (*i.e.*, time-dependent metrics), and are obtained from a static, steady state problem at each new panel orientation. It has been demonstrated that quasi-unsteady techniques can provide adequate predictive capability for moving bodies with large inertial properties that start from rest and undergo moderate acceleration[4,5,6]. This approach is attractive due to the relatively large computational expense of performing fully coupled, time-dependent, moving body simulations. This is especially true when there is a need to examine the effect of many different variables in the form of a Monte Carlo type approach. In the case of the panel jettison event, the panel inertia is large and unsteady effects are not expected to be significant, at least during initial motion while the panels are in close proximity to the SLS Center Body. Comparison of the sequential-static approach to a fully-coupled, time-dependent, viscous, moving body simulations (presented later in this paper) indicate that unsteady effects are minimal for the panel jettison event.

A number of viscous comparison simulations have been performed to access the accuracy of the inviscid simulations and provide a basis for uncertainty estimation. These simulations were obtained using the Loci/Chem[7,8] unstructured Navier-Stokes CFD solver. The inviscid results show good agreement with the full Navier-Stokes simulations during all three phases of the panel jettison event modeled by the database.

Further testing of the interpolated aerodynamic coefficients in the database was accomplished by coupling the data and MATLAB® scripts with a 6-DOF package and comparing the results to Mclaurin Aerospace's QUICDyn simulation utility. QUICDyn (Quasi Unsteady Inviscid Dynamics) loosely couples a 6-DOF solver with Cart3D to perform sequential-static moving body simulations. The results are presented in this paper, and show excellent agreement. This paper builds upon past work performed by the authors, and additional detail for certain aspects can be found in reference [9].

II. SM Panel and Vehicle Geometry

The SLS SM panel database consists of aerodynamic coefficients generated for use by the Orion MPCV Program to analyze the SM panel jettison event. The primary goal of the panel separation database was to create a tool that could be coupled with a 6-DOF dynamics model to predict SM panel separation from the SLS in a time efficient manner.

Figure 1 and Figure 2 show the SLS outer mold line (OML) used in the CFD simulations with the panels opened at 45° on the hinge. The model includes the Launch Abort System (LAS) tower and LAS thrusters and the Center Body engine fairings and nozzles. Other protuberances on the Center Body were neglected. The effect of the neglected protuberances is expected to have minimal impact on SM panel aerodynamic loads. Figure 3 provides additional details of a SM panel.

Figure 1. Side view of SLS Center Body geometry with panels open at 45° on hinge.

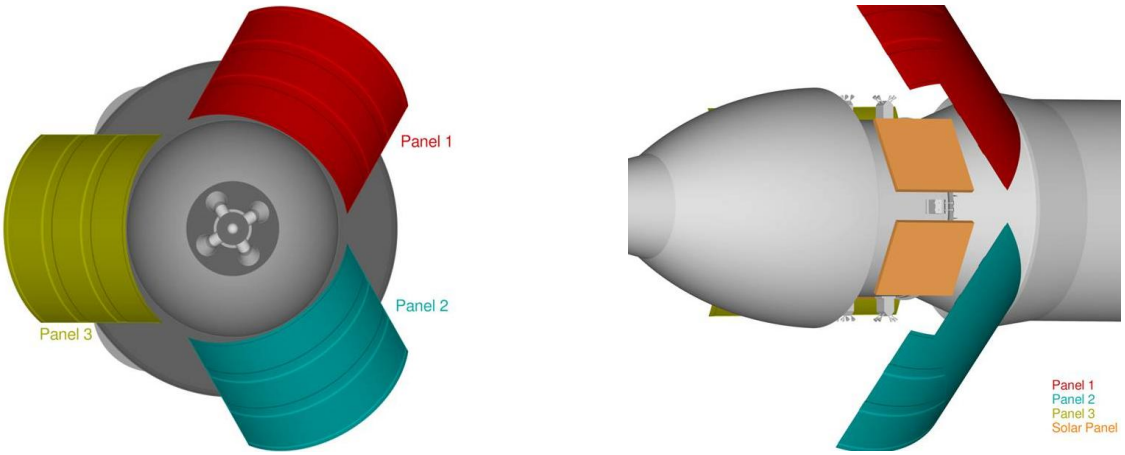

Figure 2. Front view of SLS Center Body geometry (left) and close up of internal cavity geometry (right) with panels open at 45° on hinge.

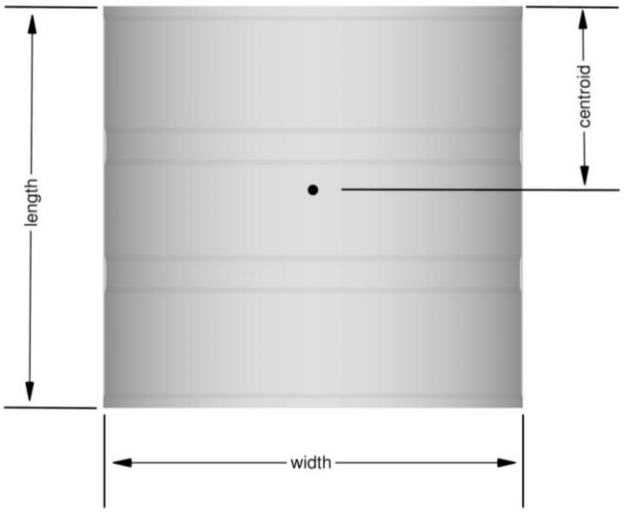

a. Top View

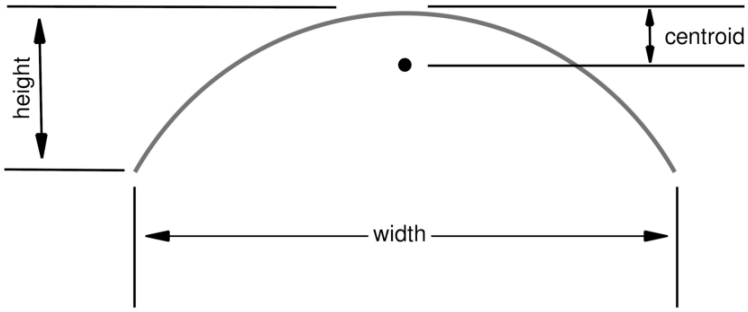

b. Front View

Figure 3: Panel Geometry

III. CFD Solver

All simulations utilized in this database were obtained from the Cart3D inviscid Cartesian CFD solver. The adjoint adaptation capabilities of Cart3D were used for each of the three zones (*i.e.*, hinged, near proximity, and far), though the number of adaptations varied between each zone. For all three zones, the adaptation functional was a composite of the force components on each of the three panels, equally weighted. The goal was to obtain meshes in excess of 3 million cells for each simulation. Depending on the panel orientations and proximity to the body, some mesh sizes exceeded 6 million cells. As an example, Figure 4 shows pressure contours for a case in the Near Proximity zone with the panels pitched 30° from the baseline orientation. The adapted mesh for this case was approximately 5.2 million cells.

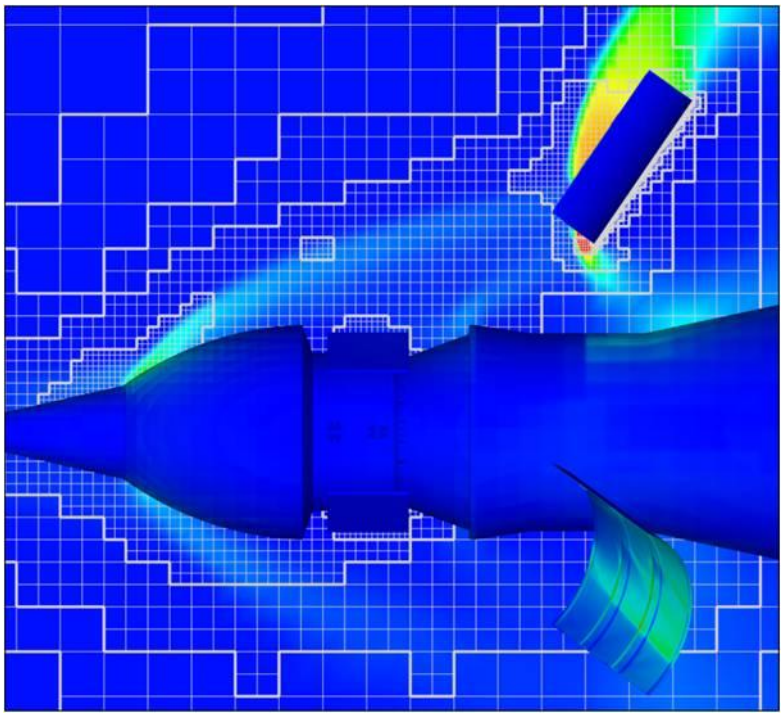

Figure 4. Pressure contours for a near proximity case with panels pitched 30° from baseline orientation

The validation and verification simulations were performed using the Loci/Chem unstructured Navier-Stokes CFD solver. The simulations were obtained using a hybrid Roe/HLLE scheme with second order spatial accuracy and steady-state time integration. The turbulence model used was the Wilcox 2008 two-equation K-omega turbulence model with Wilcox compressibility correction. Despite the complex multi-body geometry, both inviscid and viscous simulations exhibited good convergence and significant oscillations in the forces and moments on the panels were not observed.

IV. Database Development Approach and Methodology

The database is divided into three zones, shown in Figure 5. Development of the database involved prediction of the aerodynamic coefficients (generated with CFD analysis) for the SM panel during all phases of the jettison event. Initially, the panels rotate about the aft edge on two hinges until release from the SLS body at approximately 65 degrees rotation. This region is referred to as the hinged zone, and panel-to-panel and Center Body aerodynamic effects are important. The panels then travel some distance over the SLS body conical diameter expansion from the upper stage to the core stage. This region is referred to as the near-body zone. In this zone panel-to-panel effects are neglected, however, the Center Body aerodynamic effects are still included. Finally, as the panels move further from the body, the panels are modeled independently with no Center Body or panel-to-panel effects. This region is referred to as the far zone.

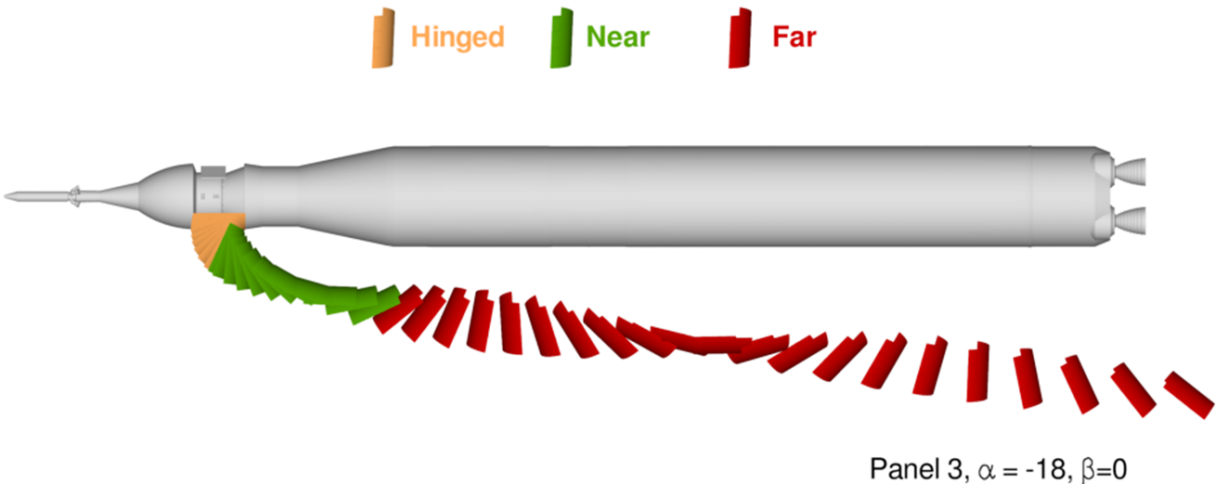

Figure 5. Displays the three database zones, hinge (orange), near proximity (green), and far/alone (red)

The bounds of the SM panel database, in terms of vehicle free stream conditions, were determined based upon trajectory data provided by NASA MSFC Guidance, Navigation and Control (GNC) and are shown in Table 1. For brevity, those details are not covered in this paper, but can be found in reference [9].

Mach number	7.0	
Angle-of-attack, deg	−25.0	−15.0
Sideslip angle, deg	−5.0	5.0

Table 1. Bounds of the SM Panel Database

Figure 6 provides panel orientation with respect to angle of attack and sideslip. The release of the SM panels happens at an approximate vehicle angle of attack between -15 and -25 degrees. Upon separation activation, a spring impacts the front of the panel and stays engaged for approximately the first 15 degrees of panel travel, with the aft end of the panel affixed to rotation about a hinge for approximately 65 degrees.

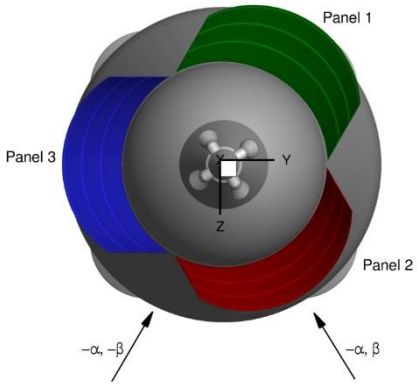

Figure 6. Panel Orientation with respect to angle of attack (α) and sideslip (β)

There is a desire to jettison the panels at the lowest altitude possible as this provides significant mass-to-orbit savings. Initial studies of the SM panel separation event demonstrated that prediction of panel trajectory at expected flight conditions using a panel alone model (*i.e.*, ignoring the presence of the SLS body) resulted in overly conservative panel trajectory predictions. When the SLS body aerodynamic effects are considered, there exists an altitude at which the aerodynamic effects on panel separation are beneficial. As the panel begins separation with a rotation about the aft-panel hinge, the cavity on the Center Body beneath the panel rapidly pressurizes, increasing angular momentum imparted to the panel. This effect results in an increased distance of clearance by the panel from the body when compared to trajectory predictions made while neglecting the SLS body. Countering the positive influence of the pressurized cavity is the force exerted by the freestream flow on the windward panel which moves it in the direction of the body. There exists an optimal separation altitude in which panel trajectory benefits in regard to body clearance from a pressurized cavity are not overcome by the freestream windward force. Figure 7 shows trajectories of the center of gravity (CG) for the windward panel modeled with and without the presence of the SLS body. As can be seen, ignoring the body results in significantly less clearance to the body. Figure 8 shows the corresponding panel orientation predictions for the windward panel.

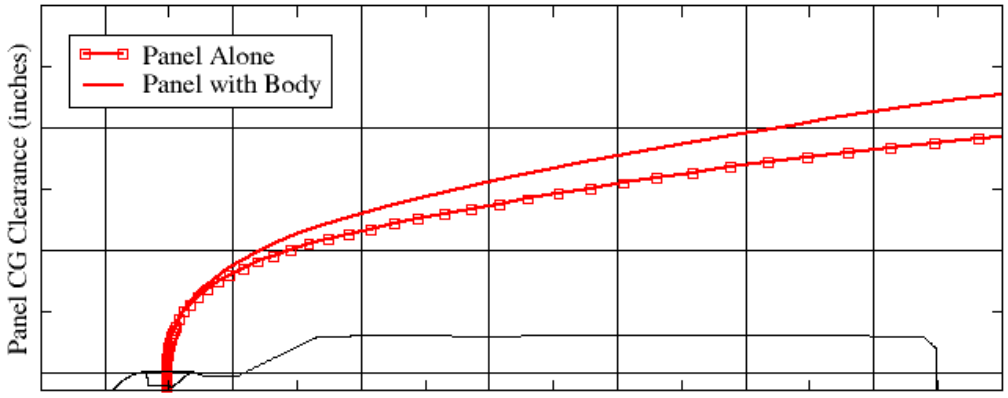

Figure 7. Panel trajectory predictions: Panel alone vs panel with inclusion of SLS Body

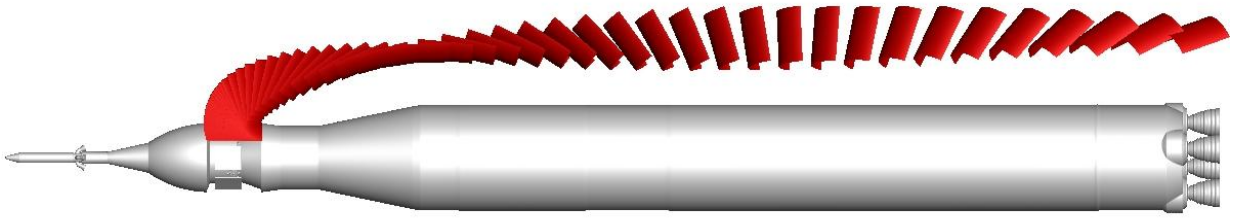

(a) Panel 2 with body aerodynamic effects

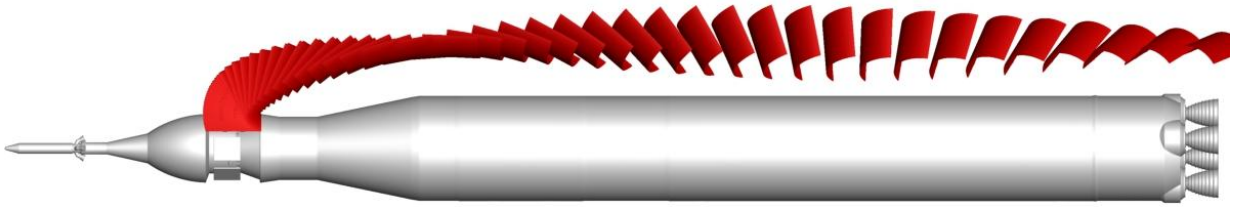

(b) Panel 2 alone – No body aerodynamic effects

Figure 8. Panel trajectory predictions: Panel alone vs panel with inclusion of SLS Body.

It should be noted that panel 2 is the windward panel and would be expected to most likely make recontact with the vehicle after jettison. As a result, it will be the panel most referenced in this paper. This is illustrated in Figure 9 which shows QUICDyn CFD predictions for the closest point to the Center Body for all 3 panels upon separation when subjected to freestream flow with the vehicle at negative angle of attack. Windward panel 2 is the only panel which moves towards the body after release from the hinge, while panels 1 (leeward) and 3 (side) are pushed away from the body.

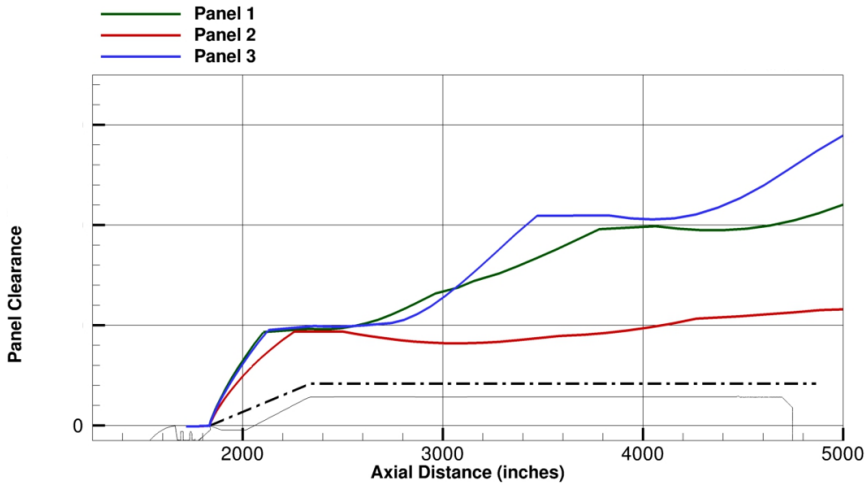

Figure 9. Panel CG Trajectories at High Angle of Attack

A. Hinged Data

This section discusses the CFD data for panels on the hinge during the initial phase of separation. In this case the aerodynamic conditions (*i.e.*, vehicle angle of attack and side slip), Center Body aerodynamic effects, and panel-to-panel influences are important. The goal is to provide 6-DOF force and moment coefficients for use when the panel motion is constrained to rotation about the hinge. Figure 10 provides a schematic of the hinge point and hinge axis definition for a panel.

The hinged panel geometric matrix is described by the following:

- Panels are rotated about the hinge axis (in the Local-Panel -θ_z direction) from 0° to 65° by 5° increments.
- A maximum of 15° difference in rotation angle is allowed between any two panels.
- For rotation angles of 0°, 5°, and 10° the panel angles are not allowed to vary from each other. In the initial design, the spring operated over approximately 15° of rotation. During this time panel motion is dominated by the spring forces, and the rotational angle will not vary significantly from panel to panel.
- The deflection angle for each panel is used to query the database for the hinged panel dataset.

The geometric matrix yields a total of 362 CFD simulations per aerodynamic condition. The six aerodynamic conditions (*i.e.*, α/β combinations) and 362 geometric conditions result in a total of 2,172 simulations for the hinged panel dataset.

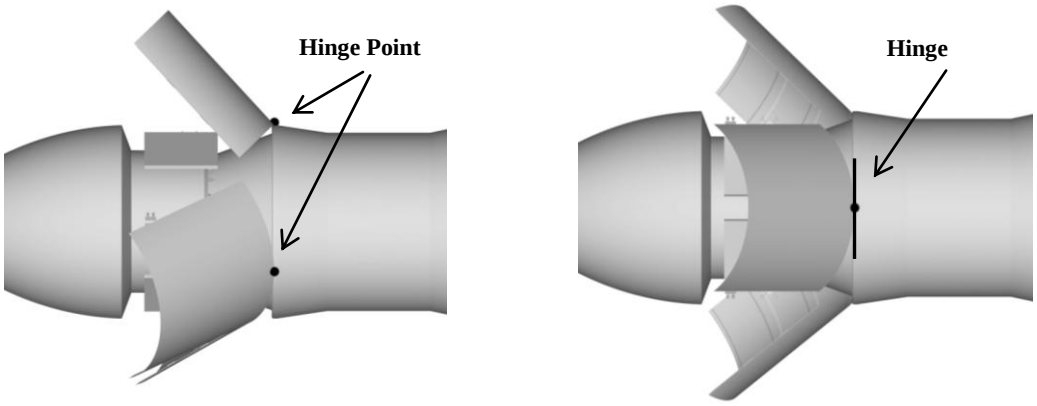

Figure 10. Panel hinge point and hinge axis

For comparison, SM panel aerodynamic coefficients from the database were plotted against Cart3D CFD data from analysis performed for the NASA Ares configuration, which utilized a similar SM panel design as SLS. Though the vehicle angle of attack varied by 2 degrees between the two vehicles for this comparison, a sample plot of the hinge moment coeffects between the two sets of data are shown below in Figure 11. What we notice for the SLS data, shown as purple circles, is a spread in the data at 10 degrees which becomes most pronounced at 25 degrees, then begins to diminish such that by 65 degrees all data points lie close together. This spread represents the panel-to-panel aerodynamic influence, as the database includes 37 unique combinations of adjacent panel rotations due to the variant freestream force acting on each panel as it rotates about the hinge. Figure 11 shows that the panel to panel influence maximizes for the windward panel at this vehicle angle attack and sideslip at 25 degrees rotation about the hinge, and is nearly zero by the time the panel reaches 65 degrees rotation.

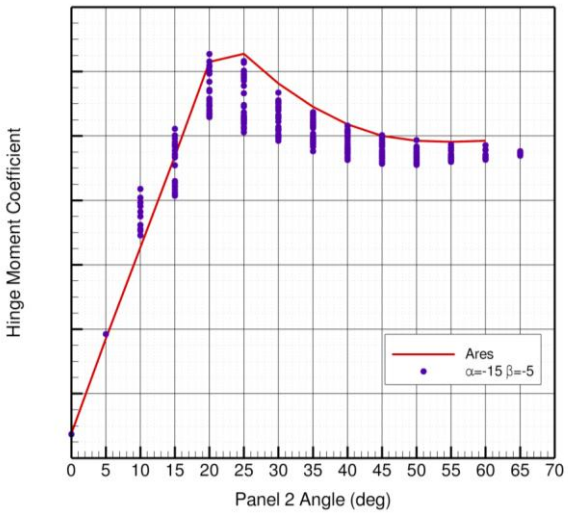

Figure 11. Comparison of Panel Hinge Moment Data between Ares and SLS

As the SM panel begins to rotate and the opening to the cavity beneath the panel is small, it would be expected to observe the most difference between the inviscid and viscous solutions. The boundary layer is influential for those cases and the cavity physics are complex. Table 2 shows the percentage difference in the predicted SM panel hinge moment between the inviscid and viscous solutions for panel 2. Data is shown for the three panel rotation angles varying from 10 to 60 degrees. While the average differential shown in the table is 7.39%, the average percent difference for rotation angles 20 degrees to 60 degrees is 3.56%. Further, while the percentage difference between schemes is large for the first 15 degrees of panel rotation, the spring exerts approximately five times the force on the panel as that of that resulting from freestream aerodynamics integrated over that period. By the time the panel aerodynamic force becomes dominant for hinge moment, the panels have sufficiently opened such that the difference between the inviscid and viscous simulations is small.

Panel Rotation in Degrees (P1-P2-P3)	% Difference between inviscid and viscous
10-10-10	25.9%
15-15-15	19.5%
20-20-20	5.7%
25-25-25	4.3%
30-30-30	2.8%
35-35-35	3.3%
45-45-45	4.0%
50-50-50	0.5%
55-55-55	3.3%
60-60-60	4.6%

Table 2. Panel 2 hinge moment coefficient comparison for alpha = -21, beta = 5

B. Near Proximity Data

This section discusses the CFD data for panels in the near proximity zone where the panel is off the hinge, but SLS Center Body aerodynamic effects are still considered important. The goal is to provide 6-DOF force and moment coefficients for use when the panel is off the hinge, but still in close proximity to the SLS Center Body.

The near panel dataset is described by the following:

- Nine panel stations; (3 axial stations) x (3 radial stations) as shown in Figure 12.
- There are 7 pitch orientations at each station; with θ_z ranging ±45° from the baseline in 15° increments.
- There are 3 roll orientations with θ_x at 0° (*i.e.*, the baseline) and ± 10° from the baseline.
- There are 3 yaw orientations with θ_y at 0° (*i.e.*, the baseline) and ± 10° from the baseline.

Each of the 9 stations has a deflection matrix of 63 simulations (pitch, roll, and yaw), resulting in a total geometric matrix of 567 simulations. Combined with the six aerodynamic conditions, the total near proximity matrix contains 3,402 simulations. The baseline stations were determined from an average of quasi-steady Cart3D/6-DOF simulations with QUICDyn. The flight conditions of the Cart3D quasi-steady simulations were determined from trajectory data provided by NASA MSFC Guidance, Navigation and Control (GNC) shown in Table 1. By predicting panel trajectories at each of the database bounding conditions ([α, β], [-α, β], [α, -β], [-α, -β]) with the QUICDyn tool, resultant bounding orientations of the panels at the nine near-body positions were determined, then margin on those panel Euler angles was added. Referring to Figure 12, stations S11, S21, and S31 are the average Cart3D/6-DOF predicted panel orientations at those axial stations. Three additional stations were included at an increased radial distance of half the panel length from the centerline. An independent review of the database was later performed by NESC (NASA Engineering and Safety Center), and a Monte Carlo analysis determined that due to changes in panel mass after the database was concluded, that three interior stations should be added to prevent possible panel aerodynamic coefficient extrapolation. These axial stations are depicted as S13, S23, and S33.

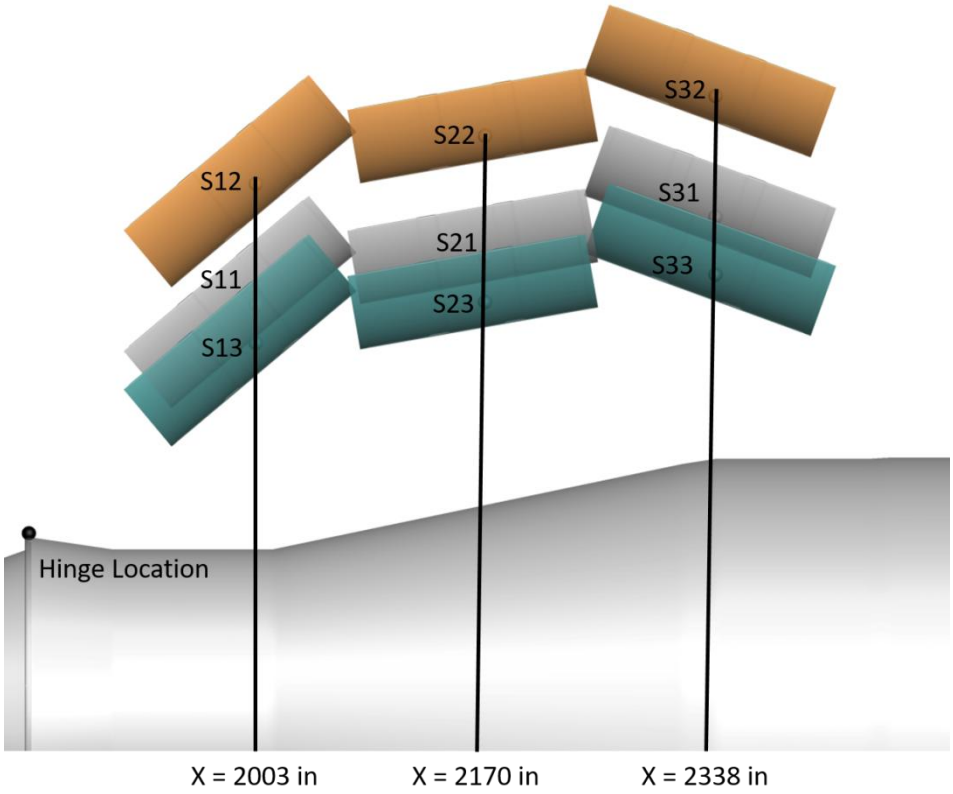

Figure 12. Additional near proximity radial stations (shown as blue) for revision 1 of the database.

Figures 13 through Figure 15 show the perturbations of the panel angles about the baseline for each station. Figure 13 shows all of the pitch perturbations for station S11. The baseline orientation is shown in pink with the perturbations shown in yellow. The pitch varies ±45° from the baseline in increments of 15°. Figure 14 shows all of the roll perturbations for station S11. The pink panel in Figure 14 is the baseline orientation, the yellow is the +10° roll, and the blue panel is the -10° roll. Figure 15 shows the same information for the yaw. It was noted that the ±10° roll and yaw perturbations encompassed all of the roll/yaw orientations (within the panel Near Proximity X regime) predicted by the Cart3D/6-DOF simulations.

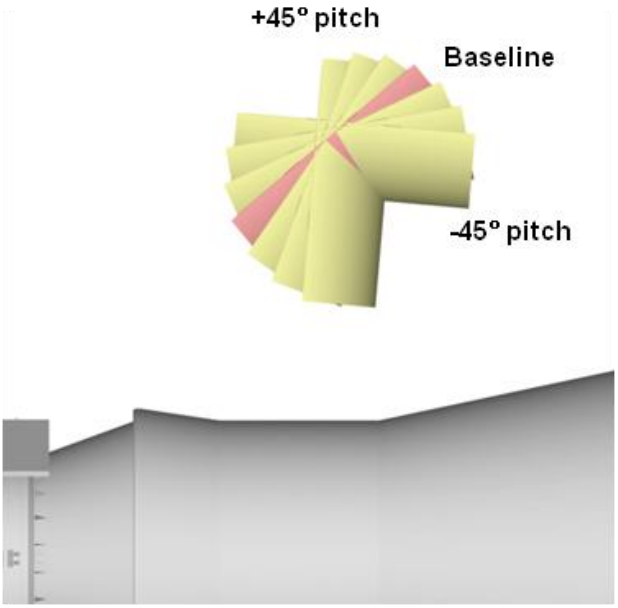

Figure 13. Euler angle pitch deflections from baseline for the Near Proximity cases.

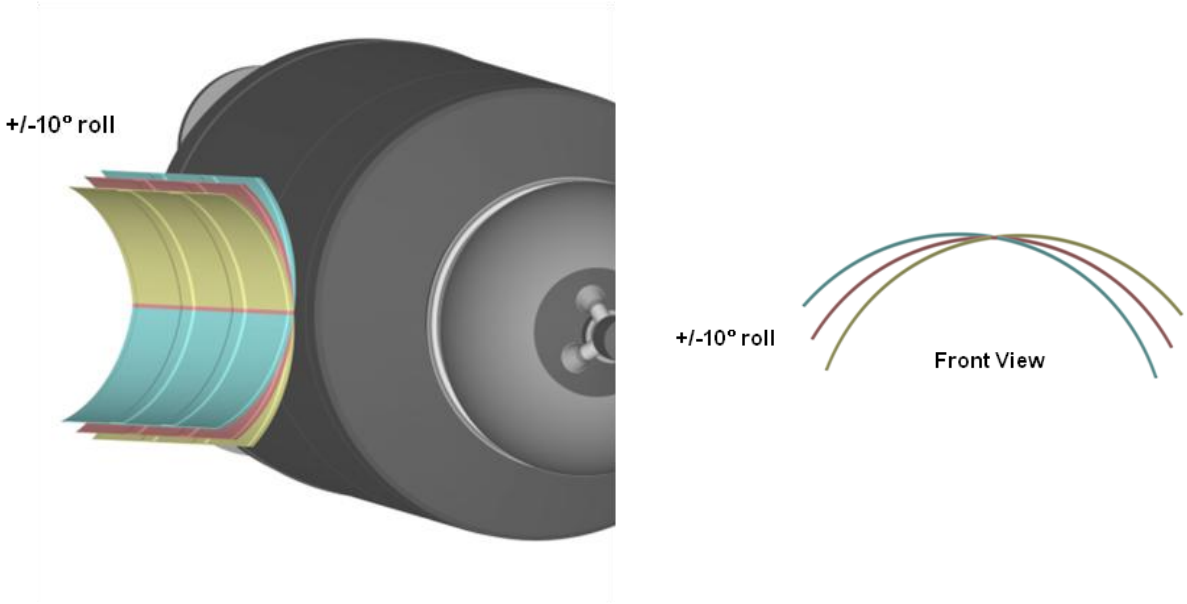

Figure 14. Euler angle roll deflections from baseline for the Near Proximity cases.

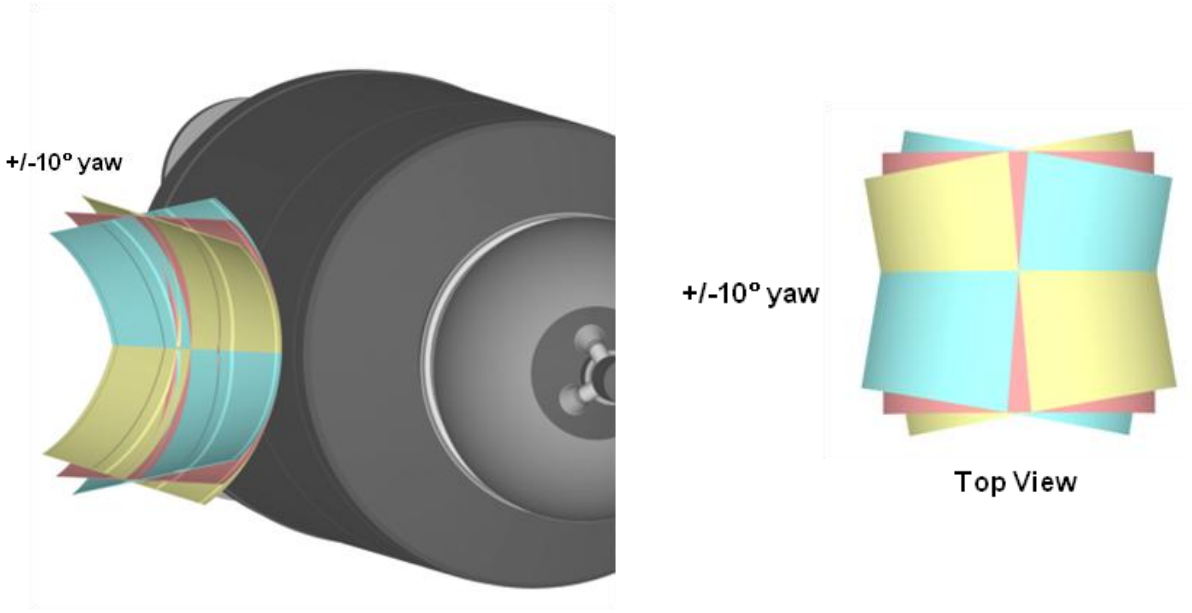

Figure 15. Euler angle yaw deflections from baseline for the Near Proximity cases.

Panel orientation is determined relative to each panel's local coordinate system as shown in Figure 16. Panel force and moment data is computed for each panel and returned in the SLS coordinate system also shown in Figure 16. An example of the data from this database is provided in Figure 17, which shows Cfy versus pitch angle for panel 2 at station S11. Note that every data point for Panel 2 is shown in this figure. The spread of the data for a given panel pitch angle is due to the different freestream conditions and the various roll and yaw orientations.

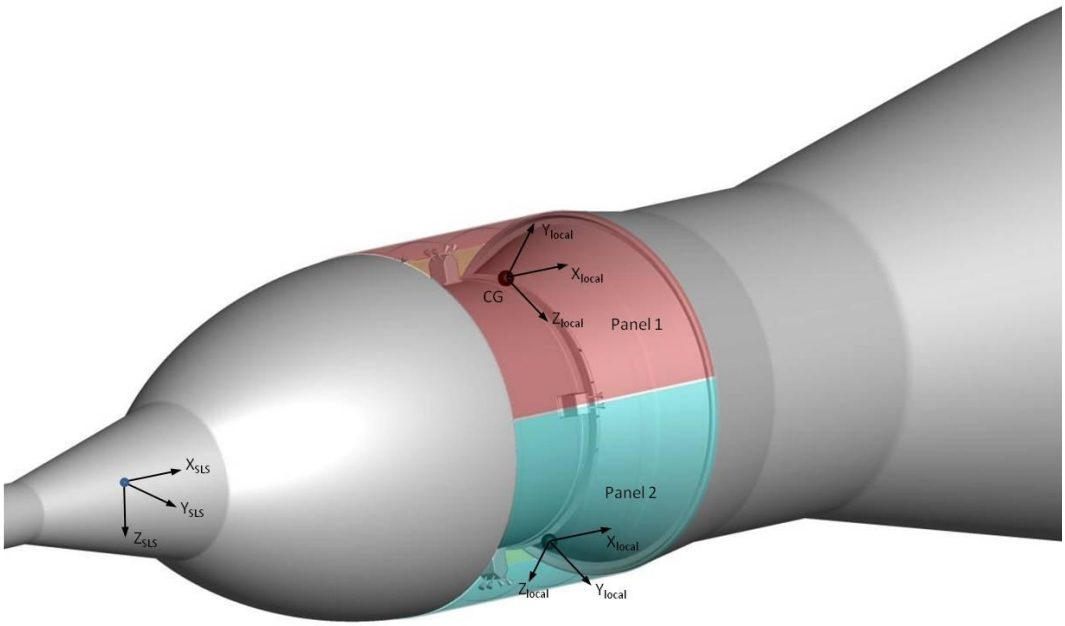

Figure 16. Local-Panel coordinate system for each panel on the SLS Center Body

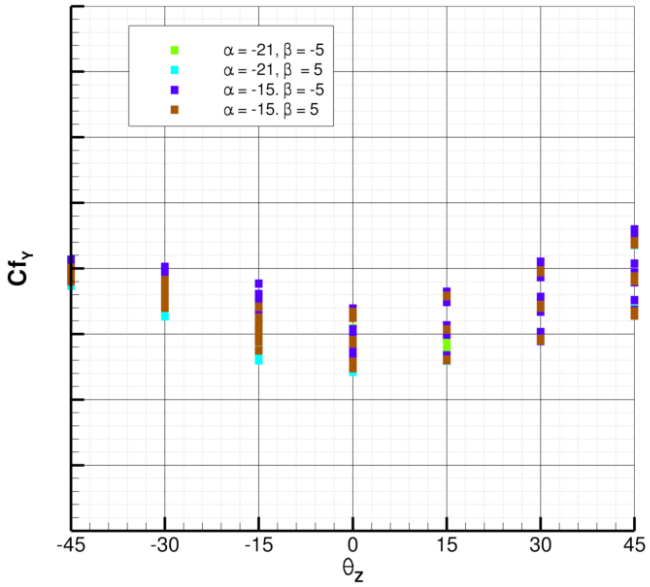

Figure 17. Panel 2 Cfy versus pitch angle for station S11

C. Far (Panel Alone) Data

This section discusses the CFD data for a panel alone in the freestream flow, without any influence from the other panels or the Center Body. The goal is to provide 6-DOF force and moment coefficients for use when the panel is far enough from the Center Body that no influence is seen on the panel aerodynamic coefficients from the body. Unlike the previous two zones, this data does not take into account the vehicle Center Body angle of attack and side slip.

The Far (Panel Alone) dataset is described by the following:

- The center of gravity of the panel is located at coordinate (0,0,0)
- All rotations occur about the center of gravity of the panel
- The Z-rotations (pitch, $\bar{\theta}_z$) are from 0 to 360 in 15° increments
- The X-rotations (roll, $\bar{\theta}_x$) are from 0 to 360 in 15° increments
- The Y-rotations (yaw, $\bar{\theta}_y$) are from 0 to 360 in 15° increments

The panel alone matrix uses the panel symmetry to reduce the number of required CFD simulations. A total of 2,184 independent CFD simulations were obtained with the panel varying in pitch from 0 to 345 degrees, yaw from 0 to 180 degrees, and roll from 0 to 90 degrees. All three rotations were performed with 15 degree increments. The CFD data was mirrored about the panel symmetry to yield a coefficient matrix of 15,000 data points in the database. Figure 18 shows the computational matrix (shown in red) compared to the full database matrix.

In order to ensure the mirroring was accurately modeling the full 360 degree matrix, a full 360° coarse matrix was performed with the CFD solver. For the coarse matrix, the three orientation angles were varied from 0 to 330 degrees in 30 degree increments. In addition, the number of adaptations was reduced by one, which produces a lower fidelity solution. Other than those two changes, the matrix was run using the same inputs as the original 2,184 simulations. A total of 1728 CFD simulations were performed for the 360 degree coarse matrix. Figure 19 shows the mirrored data versus the full coarse matrix for the z-force coefficient for all roll and yaw angles at a constant pitch angle of 120 degrees. The response curve shown in Figure 19 the fine matrix plus mirroring, the spheres show the coarse full matrix.

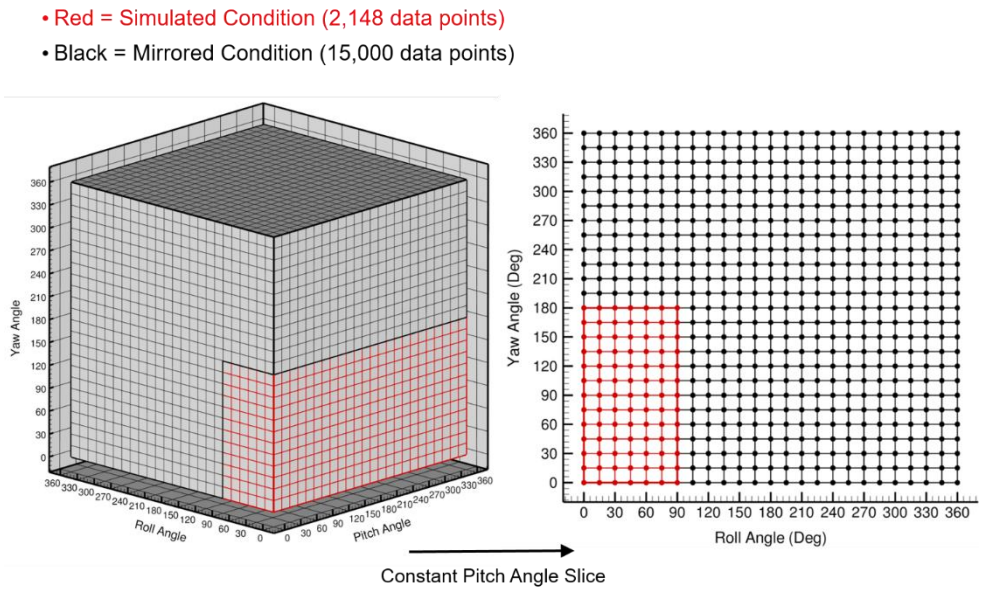

Figure 18. Computational CFD matrix and aerodynamic coefficient matrix for free panel. The computational CFD matrix is shown in red. The aerodynamic coefficient matrix provided in the database is shown in black

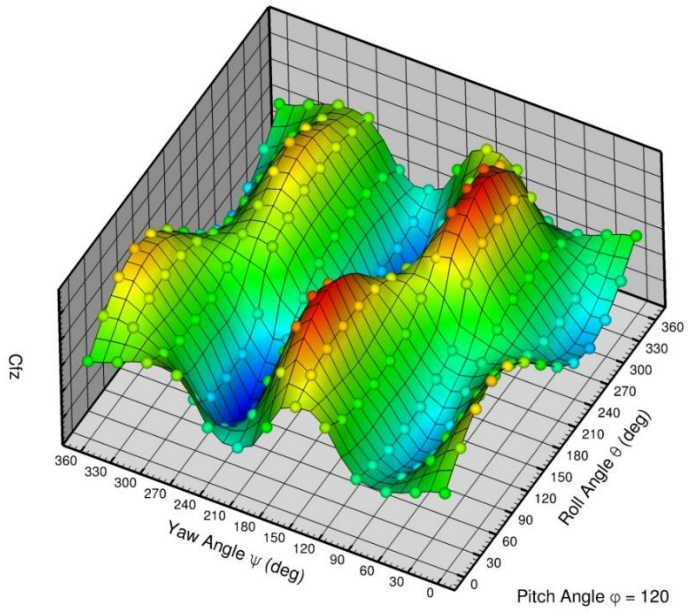

Figure 19. Example of data mirroring for the Far (Panel Alone) dataset. The case shown displays all Cfz for a pitch angle of $\bar{\theta}_z = 120°$.

D. MATLAB® Scripts

A "black box" MATLAB® code was written to query the CFD data at input values of vehicle/SM panel parameters and return the aerodynamic force and moment coefficients of the SM panels as they are jettisoned from the vehicle. While the CFD data fully defines the aerodynamics of the SM panel jettison event, the MATLAB® code provides an easy, accurate "black box" to obtain the aerodynamic coefficients for each of the panels given the multivariate nature of the CFD data. The MATLAB® functionality is divided into the same three regimes of the CFD data shown in Figure 7. The code ensures the proper function for the relevant panel flight regime. The code also contains checks of the input vehicle/panel parameters against the bounds of the CFD data and provides warnings of exceedances. Provisions have also been included to smooth transitions from one SM regime to the next with regards to the aerodynamic coefficients.

The three different flight regimes (hinged, near, and far) are dependent upon a differing number of independent variables necessitating a separate function for each zone. The code makes use of the MATLAB® function *scatteredInterpolant* for the interpolation/extrapolation of data. The function builds a response surface based on the input independent and dependent variables that passes through the input values. This response surface can be queried at desired independent variable values to determine the corresponding dependent variable value. This function can perform both two- and three-dimensional interpolation and the input data need not be evenly distributed in the data space. For example, the angles of attack do not have to be evenly incremented, nor do they have to be the same for each data point. However, because *scatteredInterpolant* can at most perform three-dimensional interpolation and the data for two of the modeled zones are functions of more than three variables, there is a need to utilize *scatteredInterpolant* more than once.

The hinged zone data is a function of five independent variables: angle of attack, side slip angle, and the three panel deflection angles. Because the value of any given aerodynamic coefficient is a function of five independent variables, multiple calls to the *scatteredInterpolant* function are required. The first step of the algorithm builds a response surface for each of the six aerodynamic conditions (a, b) for each of the three panels. This step generates eighteen response surfaces for each aerodynamic coefficient. The second step queries the response surfaces from step 1 using the user input panel deflections. For each panel this results in six values of each aerodynamic coefficient for each of the six aerodynamic conditions. These values are used to create an additional response surface that is a function of angle of attack and sideslip for each panel. This response surface is queried using the user input angle of attack and sideslip to arrive at the final aerodynamic coefficients.

The near zone is similar to the hinged zone in that the aerodynamic coefficients are a function of three position angles of the panels as well as angle of attack and sideslip for each panel, but also include the additional independent variables of radial and axial distance. Because of this similarity the function to determine the aerodynamic coefficients for the near zone follows the same logic as that for the attach zone as outlined above with the addition of logic for the added independent variables of axial and radial distance. In the first round of interpolation response surfaces are built using panel pitch, yaw, and roll angles as the independent variables for each value of angle of attack and sideslip, as well as each value of radial and axial distance for each of the three panels. There is also one additional combination of axial and radial station which represents the panel immediately after release from the hinge. Thus, after querying each of the response surfaces there are sixty values for each aerodynamic coefficient for each of the three panels. Response surfaces are now built using angle of attack and angle of sideslip as the independent variables. After querying the surface at the desired values of angle of attack and sideslip this process yields ten aerodynamic coefficient values for each panel, one value for each station as shown in Figure 12, plus the one extra station where the panel leaves the hinge. At this point these ten values are used to build a final response

surface which is queried at the desired values of radial and axial location to determine the final aerodynamic coefficients for each of the three panels

The far zone being a function of only three independent variables, pitch, yaw, and roll, requires only a single call to the *scatteredInterpolant* function. A response surface is built from the aerodynamic database data and can then be queried for any values of pitch, yaw, and roll that are input from the calling program.

V. Comparisons of the Database to Viscous Time-Accurate Fully Coupled 6-Dof Solutions

The aerodynamic coefficients provided in the database result from static, steady state simulations, and do not include the unsteady effects resulting from panel motion. As a result, use of the SM panel aerodynamic database coupled with a 6-DOF solver represents a "sequential-static" simulation. In this method, the panels are repositioned at a new time level based upon aerodynamic loads at the previous time level; however, the aerodynamic coefficients do not include the effects of panel motion (time-dependent metrics), and are obtained from a static, steady state problem at each new panel orientation. This approach is attractive due to the relatively large expense of performing fully coupled, time-dependent, moving body simulations. This is especially true when the effect of many variables need to be examined in the form of a Monte Carlo type approach. Unsteady effects are not expected to be significant due to the large panel inertias, at least while the panels are in close proximity to the SLS Center Body.

To evaluate the robustness of the database in regard to the "sequential-static" simulation approach, a fully-coupled, time-dependent, viscous, moving-body simulation was performed using Loci/Chem. This simulation utilized Chimera overset meshes and Loci/Chem's embedded 6-DOF motion model. The background mesh shown in Figure 20 was approximately 26.1 million cells. Each panel mesh (shown in Figure 21) was approximately 1.6 million cells. The combined unstructured Chimera mesh size was approximately 31 million cells. Figure 22 shows a slice through the Chimera and background meshes. To simplify the problem and in regards to schedule, the three panels were initially positioned in the 60° orientation. It was felt this was satisfactory for three reasons; first, the spring and cavity pressure dominate the panel rotation while the panel is on the hinge. Secondly, it has been shown that while on the hinge, inviscid and viscous predicted panel moments match closely for the windward panel. Finally, time-accurate moving body effects are small when the relative motion of the panels is small compared to the motion of the SLS Center Body. That relative motion begins at zero and does not become significant until the panels are free from the hinge. As a result, the effect of modeling time accurate moving bodies should be captured when starting the problem at panel release from the hinge.

The panels were given initial velocities and rotational rates consistent with the database/6-DOF simulation when the panels were at 60°. The panels were also given an acceleration in the X-direction equal to the expected acceleration of the SLS Center Body. The panels were then allowed to move unconstrained from this initial state. The time step for this simulation was 5.0×10^{-4} seconds. The simulation was run for a total time of 1.5 seconds. Figure 23 shows surface pressure contours at 0.5 seconds after the panel leaves the hinge. Figure 24 shows pressures contours on a Z-cutting plane through the Chimera and background meshes at the same time of 0.5 seconds. Figure 25 shows a close-up view of the Chimera grid peeling necessary to form the Chimera interpolation boundary. Finally, Figures 26 through Figure 28 show a comparison of panel orientations between the database/6-DOF simulation and the Loci/Chem simulation at time levels of 0.5, 1.0, and 1.5 seconds after the panels leave the hinge. The red panels are from the Loci/Chem simulation. These figures show good agreement in panel orientation between the two approaches. Figure 29 shows a comparison of the CG location and closest point for panel 2 between the database/6-DOF and fully-coupled, time-accurate Loci/Chem simulation at various times after the panel leaves the hinge. Again, the results show good agreement.

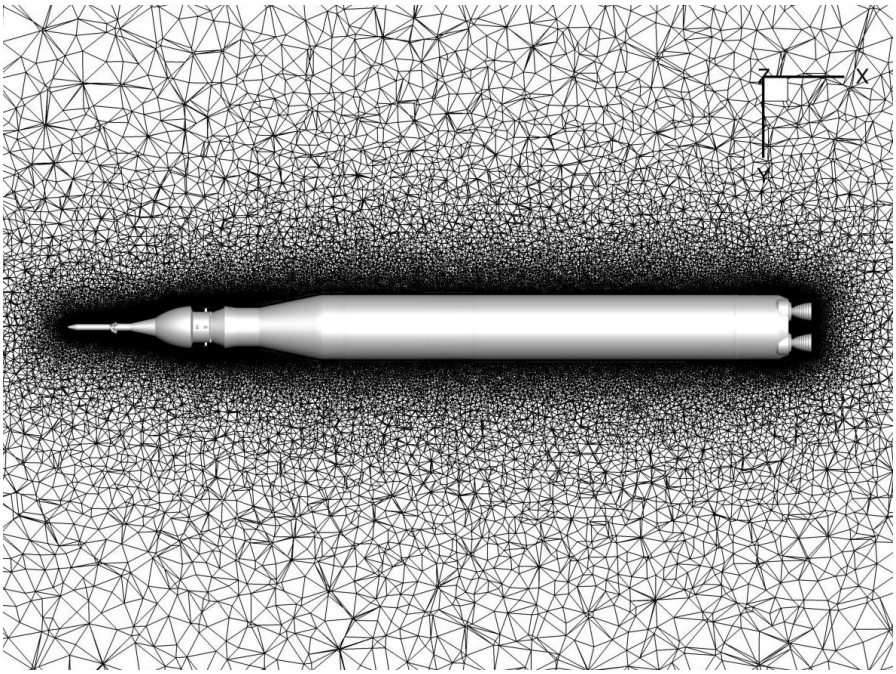

Figure 20. Chimera Background mesh.

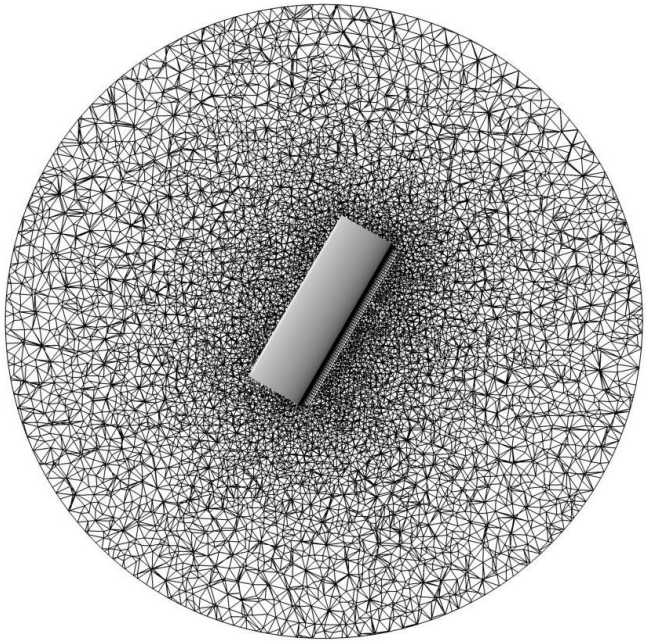

Figure 21. Chimera panel mesh.

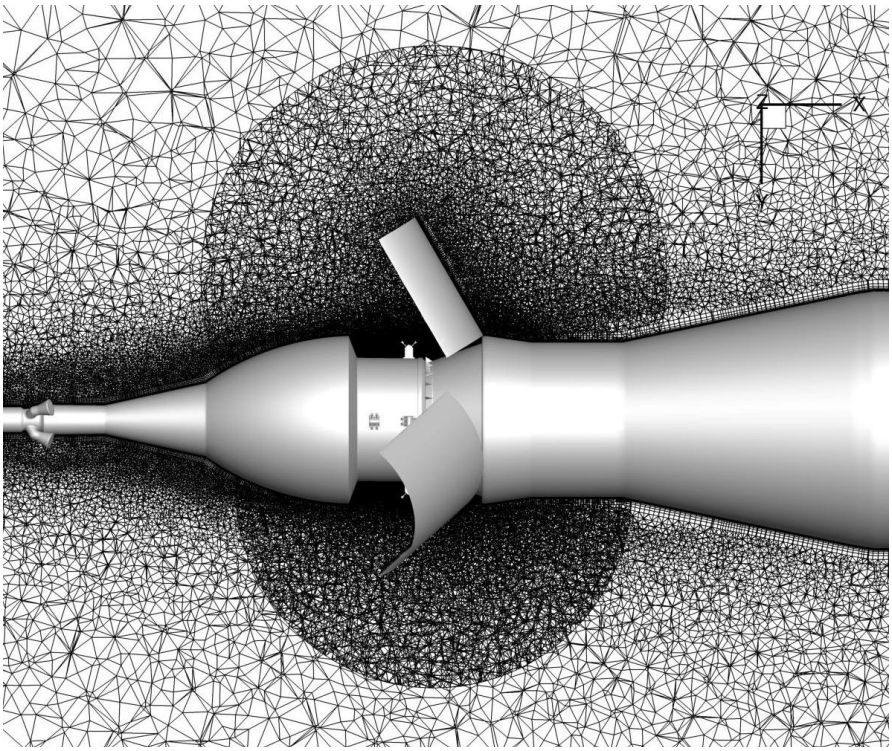

Figure 22. Z-Slice through Chimera and background meshes.

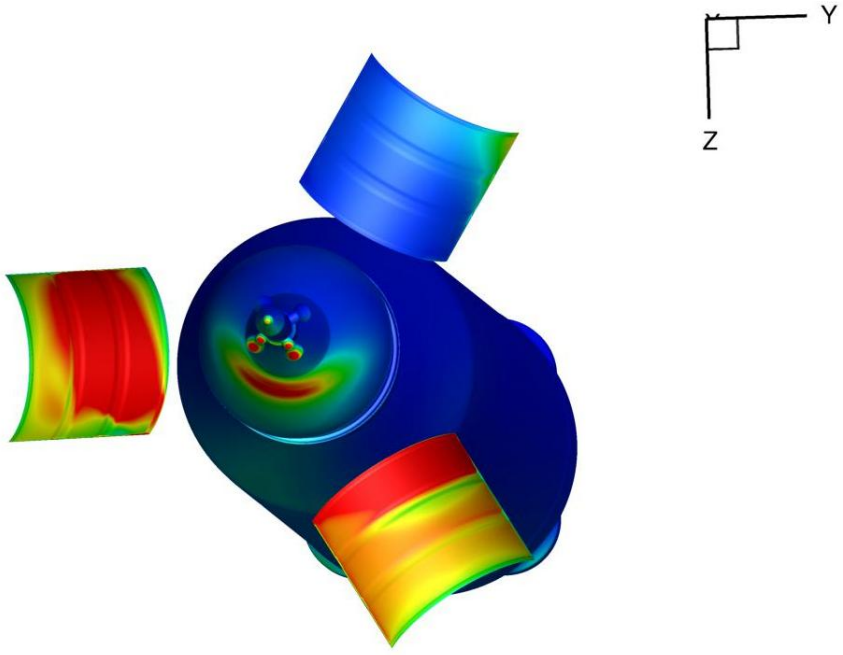

Figure 23. Pressure contours at 0.5 seconds after release from the hinges.

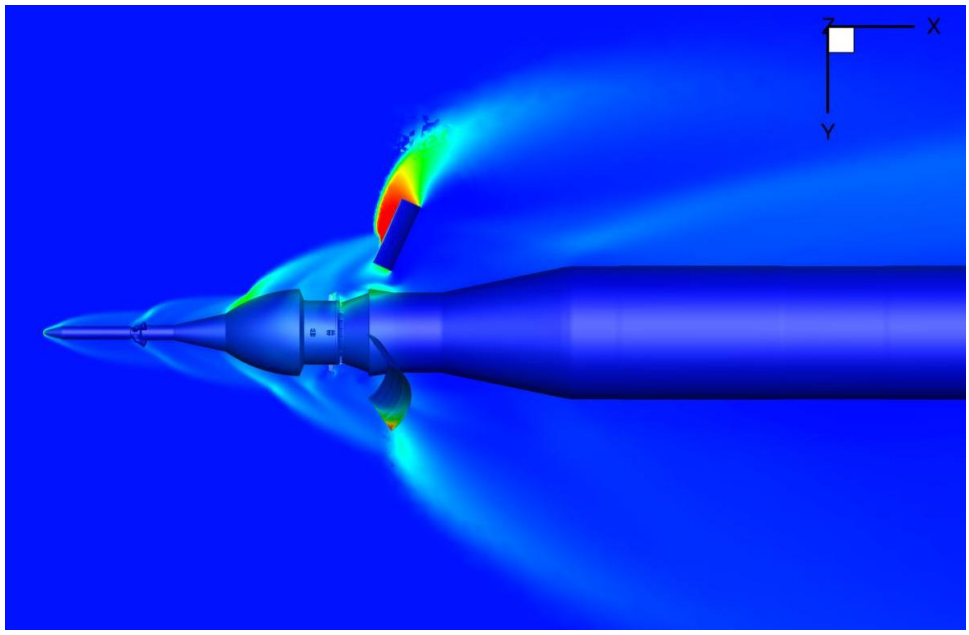

Figure 24. Pressure contours on a Z-cutting plane through the Chimera and background mesh.

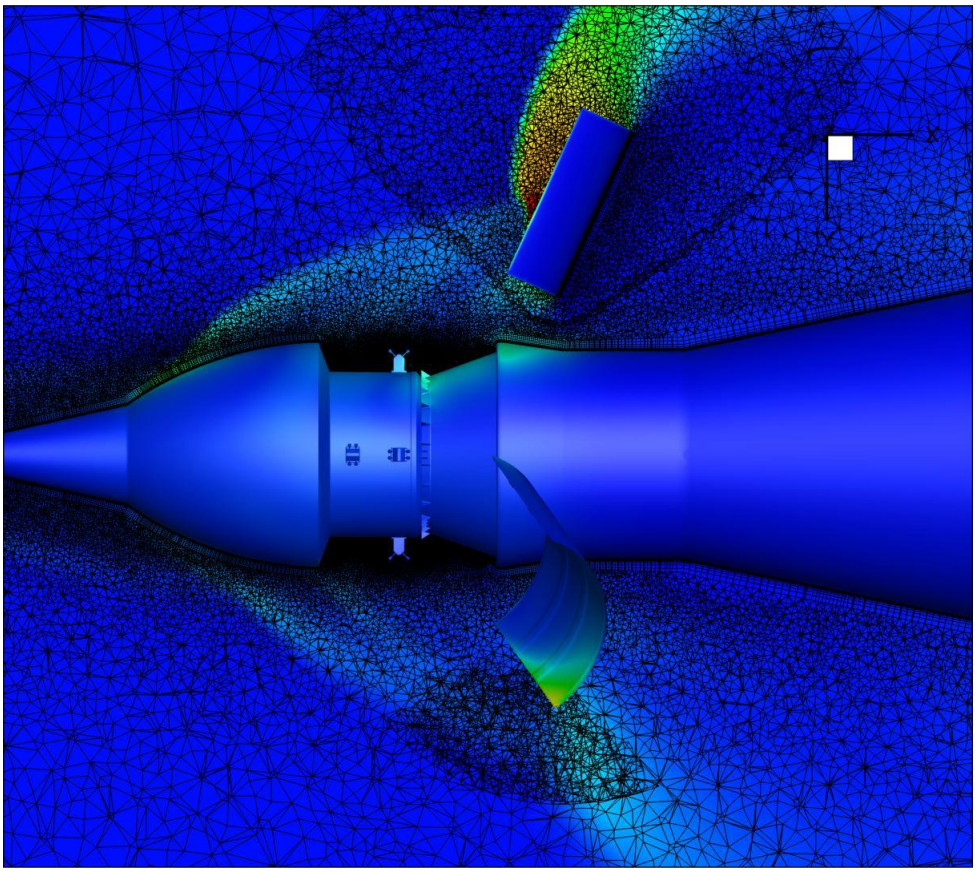

Figure 25. Close-up view of Chimera grid peeling.

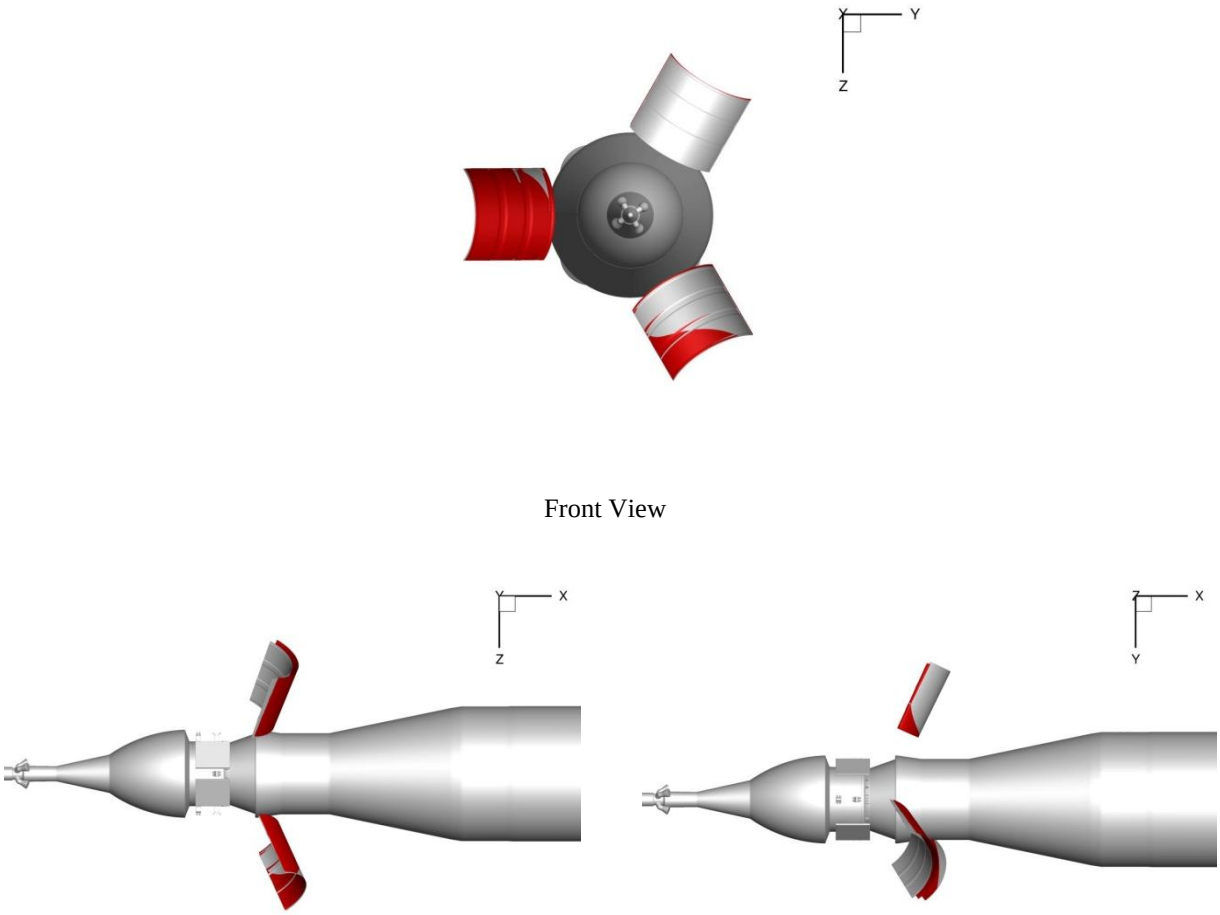

Figure 26. Panel orientation comparisons between Loci/Chem time dependent and database/6-DOF approaches. Red panels are Loci/Chem. Time level t=0.5 seconds after panel leaves the hinge.

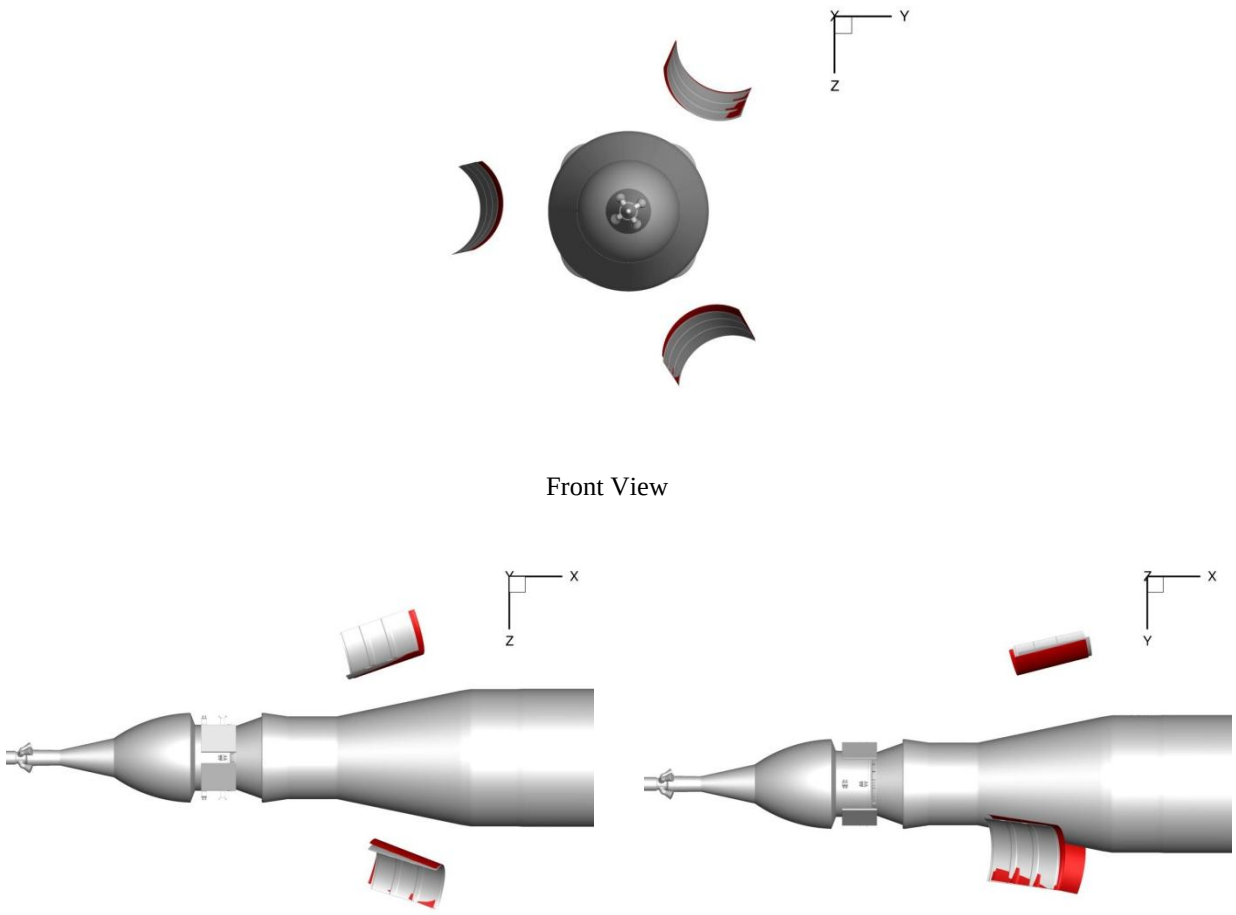

Figure 27. Panel orientation comparisons between Loci/Chem time dependent and database/6-DOF approaches. Red panels are Loci/Chem. Time level t=1.0 seconds after panel leaves the hinge.

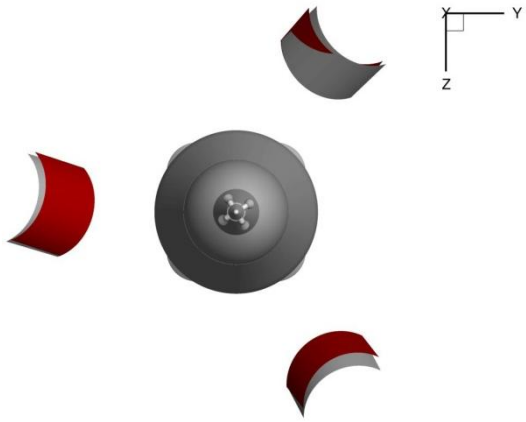

Front View

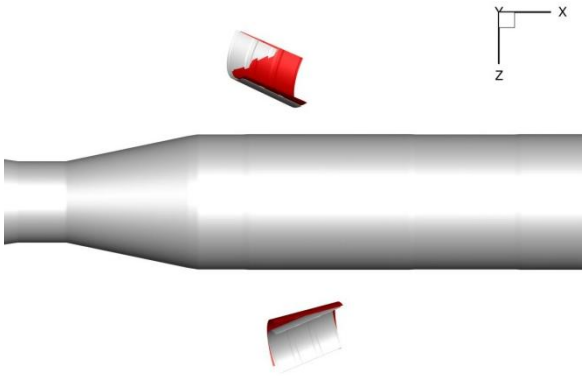

Side View

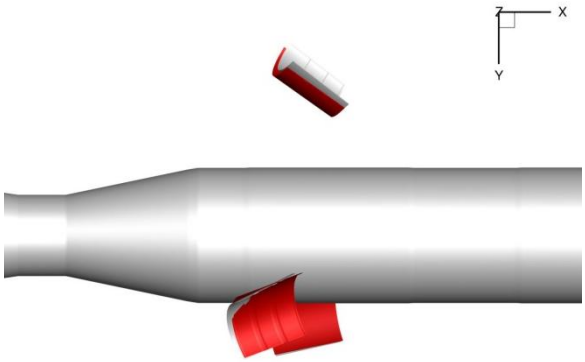

Top View

Figure 28. Panel orientation comparisons between Loci/Chem time dependent and database/6-DOF approaches. Red panels are Loci/Chem. Time level t=1.5 seconds after panel leaves the hinge.

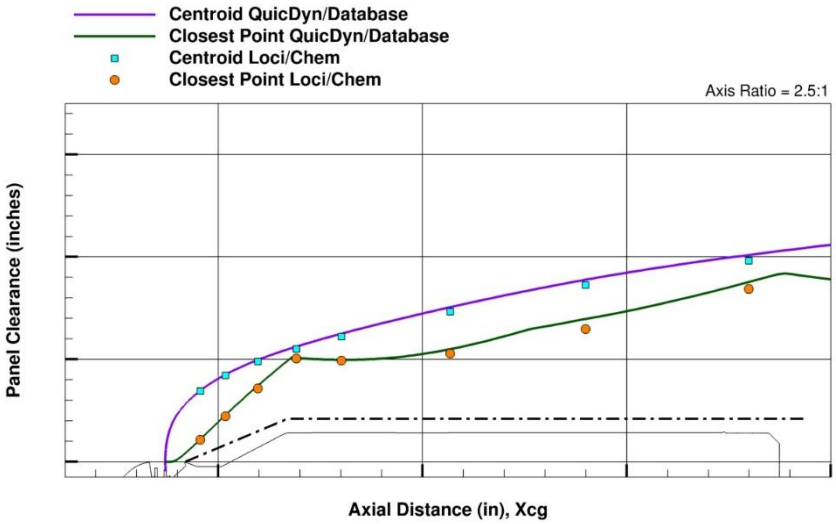

Figure 29. Comparison of panel clearance between Loci/Chem time dependent and database/6-DOF simulations.

To further assess unsteady viscous effects, a high angle of attack case of approximately three times the maximum allowable for the database was simulated. Such a case could represent an extreme event such as loss of engine. Figure 30 shows that the time-dependent 6-DOF viscous computation still agrees well with the inviscid database approach for a case where the aerodynamic effects for the windward panel are significantly more extreme than the baseline case shown in Figure 29. Additionally, this simulation demonstrates the margin available to avoid recontact.

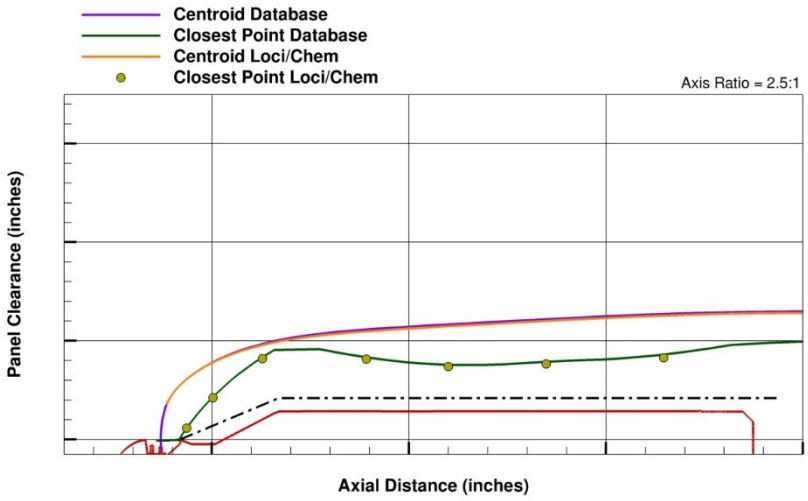

Figure 30. High Angle of Attack Comparison of panel clearance between Loci/Chem time dependent and database/6-DOF simulations.

Finally, as mentioned early in this paper, there exists a point at which the aerodynamic benefit from the cavity pressurization seen with the panel on the hinge is outweighed by the negative aspect of the freestream pressure pushing the panel back into the body. Figure 31 shows the result of running the same flight conditions as seen in Figure 30, with exception of increasing the freestream dynamic pressure by 300%. The result is the panel contacts the body roughly mid-way down the vehicle. Again, we see a close match between the viscous time-accurate 6-DOF prediction and the inviscid database trajectory, lending confidence and validity to the assumptions which form the SLS SM panel database.

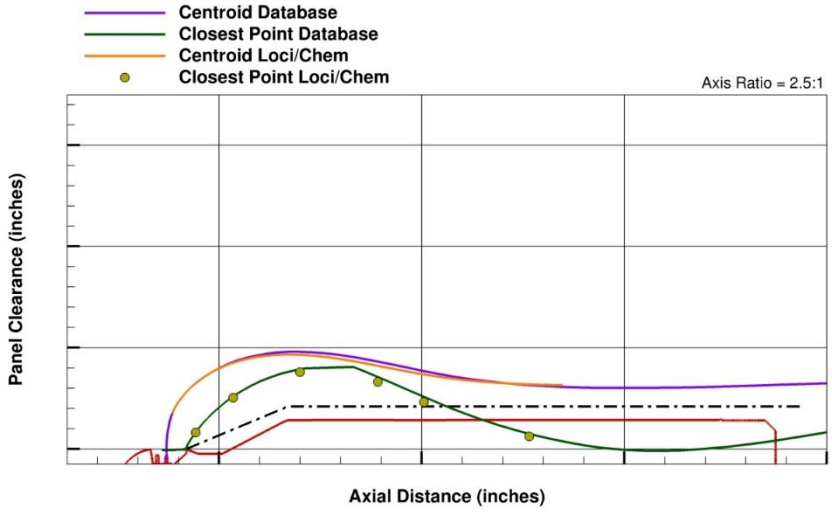

Figure 31. High Angle of Attack with 3xDynamic Pressure Comparison of panel clearance between Loci/Chem time dependent and database/6-DOF simulations

In summary, results from the time-dependent Loci/Chem simulation agree well with the database/6-DOF simulation for all cases examined. The results indicate that unsteady effects are minimal for the panel jettison event, and lend confidence that the sequential-static approach is sufficient for analysis.

VI. Uncertainty Quantification

For numerical simulations, the uncertainty can be derived from three primary sources of error: the model form error, the numerical error, and the database modeling error. The model-form error is due to neglecting certain aspects of the physical modeling. Examples include neglecting viscous and real-gas effects, and simplification of the vehicle geometry. The simulations performed for this database assumed inviscid flow with a single perfect air species. As a result, viscous and real-gas effects are neglected. Previous experience yielded confidence that it is reasonable to assume real gas effects are negligible compared to the viscous effects for these simulations. To derive a measure of the model form error, a subset of the inviscid simulations were obtained with the Loci/Chem unstructured Navier-Stokes CFD solver. Direct comparison between the viscous and inviscid CFD simulations yields a measure of the model form error. The difference in predicted force and moments between the inviscid and viscous solutions was computed. The model form error is computed from the mean of the differences plus 3-sigma of the differences. This was shown to capture all of the differences with the exception of one case which lied slightly outside the error.

The second source of error is the numerical error. Examples include the iterative convergence, statistical sampling error, discretization error, and round-off error. The numerical error for this database is computed by calculating the standard deviation of the numerical oscillations in the inviscid simulations. Due to the high volume of inviscid simulations, a mean standard deviation over all inviscid CFD simulations is used to represent the numerical uncertainty. Note, the numerical error was seen to be an order of magnitude less than the model-form errors.

The last source of error is the database modeling error. This error is primarily due to interpolation errors, response surface errors, and data manipulation assumptions (i.e. symmetry). Discrete data points are provided and linear interpolation between points is recommended if required. The error due to interpolating between data points in the database was shown to be negligible and is not presented here.

The total uncertainty is obtained by combining the model-form error estimate with the numerical error estimate. The total uncertainty is given by:

$$U_{C_X} = MI_{total}\left[UMF_{CFD}^2\{k_{num}^2(u_{C_X})_{num}^2 + k_{mod}^2(u_{C_X})_{mod}^2\}\right]^{1/2} \quad (1)$$

where subscript *num* denotes the uncertainty in the numerical error and the subscript *mod* is the uncertainty due to model form error. For the numerical error, the coverage factors (*k*) are chosen to provide 99.7% confidence of the analysis residuals for statistical sampling. The value for the numerical error coverage factor in the above equation is 3, which provides a 3-sigma variation. The physical error includes the bias plus 3-sigma variation in the differences which is already taken into account. Therefore, the physical error coverage factor is set to 1. The uncertainty model factor (UMF) is set to 1.3 as a confidence in the estimation of the physical and numerical errors. The margin index (MI) is controlled by the program and is currently set to 1.

A detailed uncertainty analysis is outside the scope of this paper. The final results and discussion of the uncertainty analysis are presented here. Each region of the database (hinged, near, and far) have separate uncertainty analysis. Due to the heavy influence of the vehicle on the hinged and near region, it was determined that a separate analysis was necessary for each panel in these regimes. However, in order to reduce the complexity of the database, the uncertainty in all regions is independent of freestream condition and panel angles. We note that this will create an uncertainty that is more conservative for the CFD conditions and panel orientations that do not drive the uncertainty model.

The uncertainty analysis for the panel hinged regime was derived from forty (40) viscous CFD simulations. These simulations placed the three panels at various orientations on the hinge. The simulations were performed at two vehicle angles of attack and two vehicle sideslip angles. Note, the hinged portion of the database provides moments about the hinge. Therefore, the forces are not used in 6-DOF simulations of the panels while on the hinge. Due to this fact, the hinged uncertainty model only provides uncertainties of the moments.

Figure 32 shows the inviscid and viscous y-component of the moment (Cmy) about the hinge for the windward panel (panel 2) for a positive and negative vehicle sideslip angle. Also shown in the plot is the uncertainty model (shown as error bars). Note that the uncertainty is independent of panel hinge angle and CFD condition. From the figure it can be seen that the largest difference between the viscous and inviscid CFD occurs at the lower panel orientations for a negative sideslip angle. These differences are the drivers for the uncertainty model. Clearly, at higher panel angles the uncertainty model is providing significant conservatism. In addition, significant conservatism is observed for the entire range of panel angles for a positive vehicle sideslip. The z-component of the moment (Cmz) for the windward panel show similar trends (not shown here).

For the near proximity regime, we expect panel to panel influences to be minimal. However, the orientation of the panels with respect to the body of the vehicle has a heavy influence. As with the hinged regime, the near proximity regime provides an uncertainty for each panel. But the model for each panel is independent of local panel orientation and CFD condition. Twenty-four (24) viscous CFD simulations were performed. The simulations were performed for the baseline panel orientation at each of the six initial panel stations (S11, S12, S21, S22, S31, and S32). Simulations were obtained at two vehicle angles of attack and two vehicle sideslip angles. Uncertainties are provided for the six force and moment components.

Figure 33 shows the viscous comparisons and uncertainty for the windward panel in the near regime for baseline orientation at station S11. The figure shows Cfx and Cmy which exhibited the largest uncertainties in the forces and moments in this regime. Similar to the hinged region, note that the uncertainty model is independent of CFD condition (shown on the x-axis). Though not visible in this plot, the uncertainty is also independent of station. As was observed for the hinged regime, for both Cfx and Cmy, the largest differences are observed at the negative sideslip condition (α=−15, β=−5).

The far panel regime provides data for the forces and moments when the panel is sufficiently far from the body and other panels, such that body-to-body influences can be neglected. Note the far panel models a single panel in a freestream. Therefore there is only a single freestream condition to be considered. Twenty-nine (29) viscous CFD simulations were obtained to arrive at an uncertainty model for the six force and moment coefficients. Three sets of viscous simulations were obtained. The first set yaws (θ_y) the panel from 15 to 180 degrees by 15 degrees while holding the roll (θ_x) and pitch (θ_z) at zero degrees. The second set of simulations pitches the panel from 15 to 330 degrees while holding the roll and yaw at zero degrees. The pitch varies by 15 degrees from 15 to 90 degrees and by 30 degrees between 90 and 330 degrees. The last set of simulations rolls the panel from 15 to 90 degrees by 15 degrees while holding the yaw and pitch at zero degrees. Figure 34 shows the Cfx and Cfy from the set of pitch simulations. Note that the uncertainties are independent of pitch angle. Overall, the inviscid solver does a reasonable job capturing the forces and moments on the free panel. The largest uncertainty occurrs for Cfx. This is expected as the x-component of force will have the largest viscous shear component due to the significant planform area.

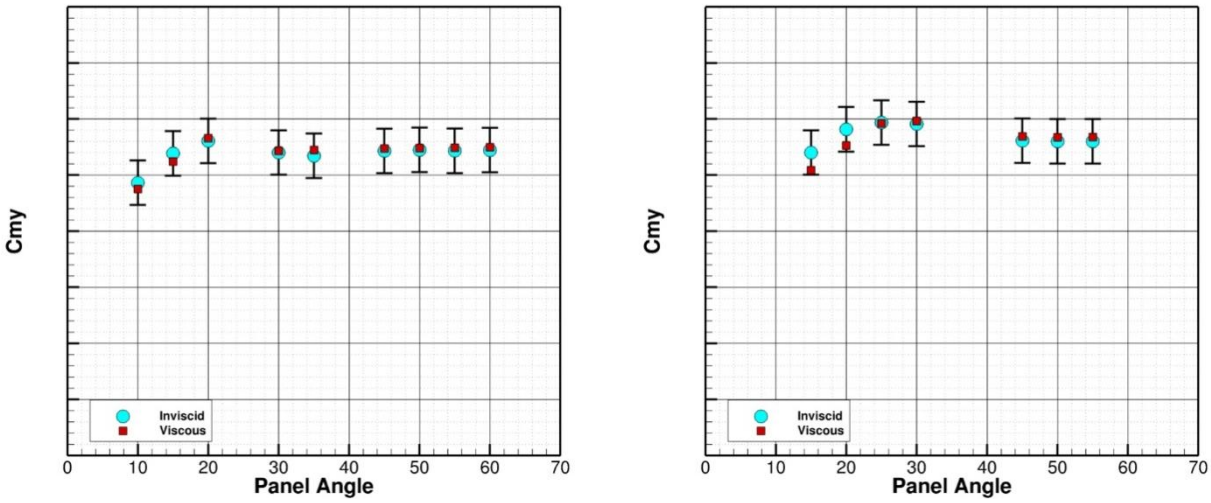

Positive Sideslip (+β) **Negative Sideslip (-β)**

Figure 32. Hinged regime viscous comparisons and uncertainties for the windward panel.

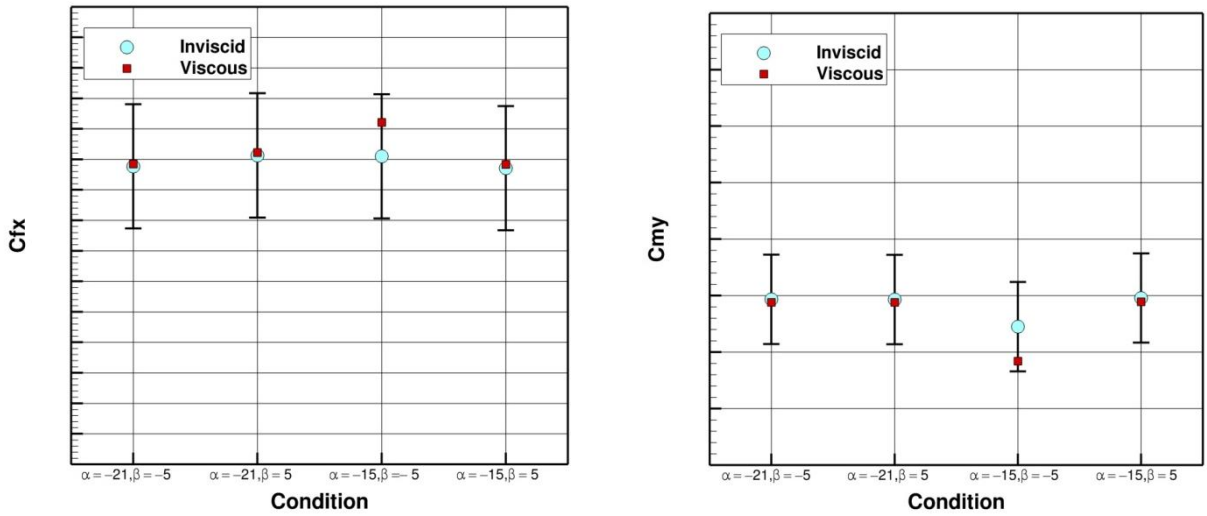

Figure 33. Near regime viscous comparisons and uncertainties for the windward panel at station S11 with baseline orientation.

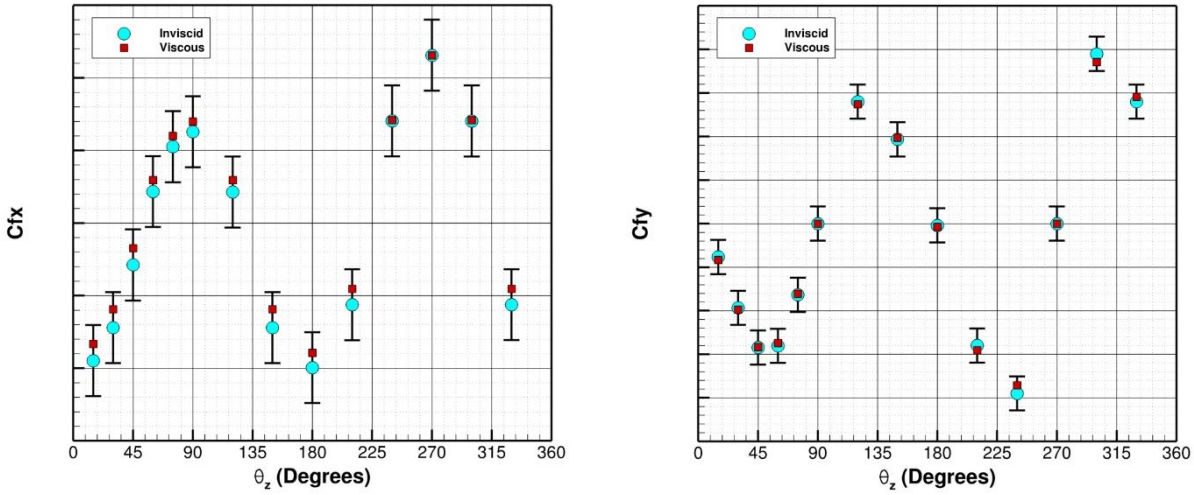

Figure 34. Far regime viscous comparisons and uncertainties versus panel pitch angle

IV. Conclusions

An approach is presented for generation of the SLS SM panel aerodynamic coefficient database. The database was generated for use by the Orion MPCV Program to perform Monte Carlo simulations of the SM panel jettison event for purpose of panel clearance analysis. The database was divided into three distinct zones; panel while hinged, panel near the Center Body and the panel-alone. Necessary database bounds were determined from trajectory data provided from the NASA MSFC Guidance, Navigation and Control group. The database coefficients were created using the inviscid CFD solver, Cart3D. The database contains a total of 7,758 CFD simulations (2,172 hinged, 3,402 near body, 2,184 panel alone). The complete database due to mirroring of solutions contains 20,574 CFD simulations.

Initial studies show the effect of the SLS Center Body cannot be neglected in panel trajectory determination. Upon initiation of the jettison event, the panel rotates about two aft hinges. During this period, the cavity beneath the panel

rapidly pressurizes and imparts significant angular momentum to the panel. This effect assists in panel clearance of the Center Body. There exists a range of altitude for which the pressurization can benefit in panel separation and overcomes the negative effect of freestream pressure pushing the windward panel back towards the Center Body.

Detailed comparisons between inviscid (Cart3D) and viscous (Loci/CHEM) simulations for all three database zones were performed. For the hinged portion of the database, results show that inviscid and viscous results compare well after the panel motion is no longer dominated by the force of the spring during initial rotation. All other portions of the database show good agreement between viscous and inviscid solutions.

An uncertainty analysis was developed by utilizing the differences between the viscous and inviscid CFD simulations to yield a measure of the model form error. The numerical uncertainty was determined using a mean standard deviation numerical oscillations over all inviscid CFD simulations. The numerical error was seen to be an order of magnitude less than the model-form errors. In order to reduce the complexity of the database, the uncertainty for all regions is independent of freestream condition and panel angles. This was shown to create an uncertainty that is more conservative for the CFD conditions and panel orientations that do not drive the uncertainty model.

The panels have large inertial properties and begin motion from rest relative to the Center Body. As a result, it was expected that the unsteady effects of panel motion were negligible. To verify this assumption, a series of time-accurate viscous 6-DOF solutions were obtained with the Loci/Chem solver to assess importance of unsteady effects. Results from the time-dependent Loci/Chem simulation agree well with the database/6-DOF approach for all cases examined. These simulations confirm that unsteady effects are negligible and that the sequential-static approach used to create the database coefficients is a valid approach. In addition high angle of attack cases demonstrate there is ample margin for nominal panel separation event.

References

[1]Aftosmis, M.J., Berger, M.J., and Adomavicius, G. “A Parallel Multilevel Method for Adaptively Refined Cartesian Grids with Embedded Boundaries”, AIAA-2000-0808, January 2000.

[2]Aftosmis, M.J., Berger, M.J., and Melton, J.E., "Robust and Efficient Cartesian Mesh Generation for Component-Based Geometry", AIAA Journal, Vol. 36, No. 6, pp. 952-960, 1998.

[3]Hall, L.H., Eppard, W.M., Applebaum, M.P., Mitchell, C.R., “Computational Simulation Techniques of Panel Fairing Jettison from a Launch Vehicle System”, JANNAF 959, 2008.

[4]Hall, L.H., Applebaum, M.P., Eppard, W.M.,"Debris Transport Modeling Techniques on Launch Vehicle Systems",49th AIAA Aerospace Sciences Meeting, Orlando, Fl, Jan 4-7, 2011.

[5]Murman, S.M., Aftosmis, M.J., Berger, M.J. “Simulations of 6-DOF Motion with a Cartesian Method”, AIAA-2003-1246, 41st AIAA Aerospace Sciences Meeting, Reno, NV, Jan 6-9, 2003.

[6]Hall, L.H., Parthasarathy, V., “Validation of an Automated Chimera/6-DOF Methodology for Multiple Moving Body Problems”, AIAA 98-0753, 1998

[7]Luke, E. A. and George, T., “Loci: A Rule-Based Framework for Parallel Multidisciplinary Simulation Synthesis”, Journal of Functional Programming, Special Issue on Functional Approaches to High Performance Parallel Programming, Volume 15, Issue 03, 2005, pp. 477-502, Cambridge University Press.

[8]Luke, E. A., Tong, X.-L., Wu, J., and Cinnella, P., "CHEM 2: A Finite-Rate Viscous Chemistry Solver – The User Guide," Tech. Rep. MSSU-COE-ERC-04-07, Mississippi State University, 2004.

[9]Applebaum, M.P., Hall, L.H., Eppard, W.M., Purinton, D.C., Campbell, J.R., Blevins, J.A., "Development of an Aerodynamic Analysis Method and Database for the SLS Service Module Panel Jettison Event Utilizing Inviscid CFD and MATLAB", 53rd AIAA Aerospace Sciences Meeting, Kissimmee, Fl, Jan 5-9, 2015.